

Accepted Manuscript

Title: Oxidative esterification of furfural by Au nanoparticles supported CMK-3 mesoporous catalysts

Authors: Ramakrishnan Radhakrishnan, Sivakumar Thiripuranthagan, Arulselvan Devarajan, Sakthivel Kumaravel, Elangovan Erusappan, Kathiravan Kannan



PII: S0926-860X(17)30341-1
DOI: <http://dx.doi.org/doi:10.1016/j.apcata.2017.07.031>
Reference: APCATA 16336

To appear in: *Applied Catalysis A: General*

Received date: 24-4-2017
Revised date: 5-7-2017
Accepted date: 20-7-2017

Please cite this article as: Radhakrishnan Ramakrishnan, Thiripuranthagan Sivakumar, Devarajan Arulselvan, Kumaravel Sakthivel, Erusappan Elangovan, Kannan Kathiravan, Oxidative esterification of furfural by Au nanoparticles supported CMK-3 mesoporous catalysts, Applied Catalysis A, General <http://dx.doi.org/10.1016/j.apcata.2017.07.031>

This is a PDF file of an unedited manuscript that has been accepted for publication. As a service to our customers we are providing this early version of the manuscript. The manuscript will undergo copyediting, typesetting, and review of the resulting proof before it is published in its final form. Please note that during the production process errors may be discovered which could affect the content, and all legal disclaimers that apply to the journal pertain.

Oxidative esterification of furfural by Au nanoparticles supported CMK-3 mesoporous catalysts.

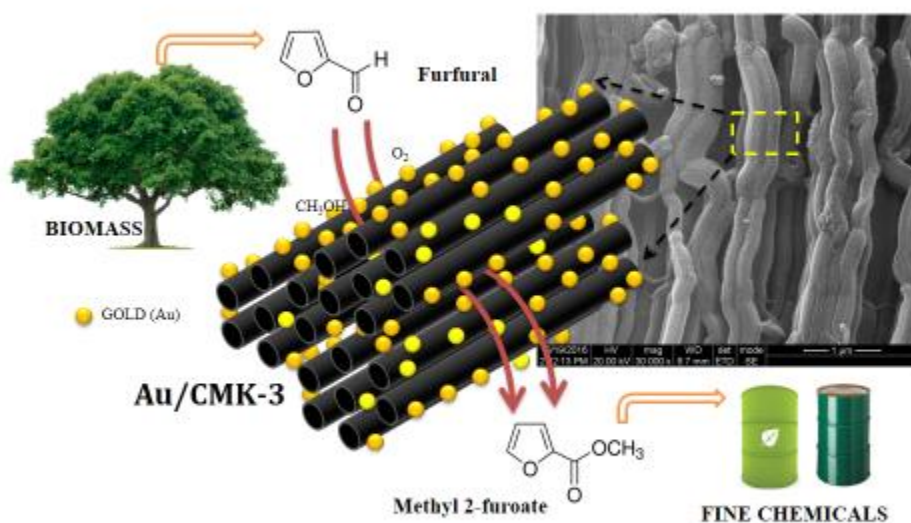
Ramakrishnan Radhakrishnan, Sivakumar Thiripuranthagan*, Arulselvan Devarajan, Sakthivel Kumaravel, Elangovan Erusappan and Kathiravan Kannan.

Catalysis Laboratory, Department of Applied Science and Technology, A.C.Tech Campus, Anna University, Chennai-25.

* *Corresponding author*

E-mail: tssivakumar@yahoo.com; Tel.: 91-44-22359193.

Graphical abstract



HIGHLIGHTS

CMK-3 was synthesized successfully from SBA-15 and sucrose via nanocasting method.

Hydrophobic Au/CMK-3 catalyst was prepared by wet impregnation in organic medium.

Among the different metals and supports, Au and CMK-3 were found to be the best.

5% Au/CMK-3 was found to be the best in the oxidative esterification of furfural.

Among the oxidants, O₂ provided high conversion (99.7%) and selectivity (99.6%).

ABSTRACT

Furfural which is derived from the hemicellulose fraction of abundant lignocellulose has received significant attention to many researchers as its valorization yields useful products such as fine chemicals and transportation fuels. Methyl 2-furoate is one of the important valorized products of furfural as it finds applications in flavor and fragrance industries. Methyl 2-furoate is generally obtained by oxidation followed by esterification of furfural but under acidic and corrosive conditions. Uniform rods of CMK-3 mesoporous materials were successfully synthesized by using nanocasting method. Au nano particles were impregnated into the pores of CMK-3 by wet impregnation method followed by hydrogen reduction at high temperature (673 K). All the catalysts were thoroughly characterized by various analytical techniques. Homogeneous dispersion of Au nano particles \approx 3nm size was found over CMK-3 materials. Qualitative and quantitative analyses of Au were made by XPS and ICP techniques. The effect of impregnating metal ions (Ni, Pt and Pd) and supports (SBA-15, graphite, graphene, MWCNT, activated carbon and TiO₂) was studied on the catalytic conversion of furfural. Among them, Au/CMK-3 catalyst was found to be the best. Among the Au/CMK-3 catalysts, 5% Au/CMK-3 catalyst showed remarkable conversion of furfural (99.7%) with very high selectivity towards

methyl 2-furoate (99.6%). The stability and reusability of the 5% Au/CMK-3 catalyst was found to be very good even after five catalytic cycles.

KEYWORDS

Mesoporous Au/CMK-3, Furfural, Methyl 2-furoate, Oxidative Esterification, Nanocasting

1. Introduction:

There is a great demand for the ordered porous materials in the area of heterogeneous catalysis, adsorption, drug delivery and electronics [1-4]. Among the ordered materials ordered mesoporous silica (OMS) and ordered mesoporous carbon (OMC) are of great interest and hence the catalyst world has seen several ordered mesoporous materials synthesized by using different soft and hard templates. The first one in the group was M41S series synthesized by Kresge et. al. in the year of 1990 [5,6]. These mesoporous silicates have uniform pore size (2-10 nm) with long range ordered nanochannels, high surface area ($> 2000 \text{ m}^2/\text{g}$) and the adjustable periodicity. To suit different applications, these OMS materials were modified either in the framework with the introduction of hetero elements or surface modification through silanol groups. A detailed information regarding the synthesis, characterization and applications of these various ordered mesoporous silica (OMS) series are found in various literature reviews [7-9]. Among the OMS materials, SBA-15 with hexagonal mesostructure synthesized by using triblock polymer has been studied extensively due to its tunable pore size (4 – 14 nm) [10].

Similarly ordered mesoporous carbons (OMC) are another group of fascinating carbon materials. They are highly ordered with uniform array of mesopores. Ordered mesoporous carbons (OMC) are generally prepared using ordered mesoporous silica (OMS) as template. Ryoo et. al. synthesized one such material using MCM-48 as template in the year of 1999 and it is referred as CMK-1[11]. OMC materials with tunable pore size, controllable pore structure, surface area,

high pore volume, conductivity and stability are generally synthesized by nanocasting method [12, 13]. Due to these unique properties of OMC, number of environmental friendly low cost energy storage and conversion devices have been developed. Apart from these applications, these materials also find greater use in the area of catalysis and gas separations. Generally the synthesis of OMC involves stepwise impregnation of carbon precursor (monomer, polymer, etc.) in the pores of mesoporous silica materials to get desired silica to carbon ratio [14]. The precursor within the pores are polymerized and carbonized in the pore structures resulting in the formation of carbon-silica composites. The resulting composite is washed with aq.HF to remove silica template to yield CMK-n. A large variety of OMC with different mesostructures such as CMK-1(MCM-48, cubic *Ia3d*) [15], CMK-2 (SBA-1, cubic *pm3n*) [16], CMK-3(SBA-15, rod type *p6mm*)[17-20], CMK-4 (MCM-48, *Ia3d*) [21], CMK-5 (SBA-15,tube type *p6mm*) [22], OMC(SBA-16, cubic *Im3m*) [23] and CMK-8 (KIT-6, rod type) [24] were prepared by nanocasting method using various carbon precursors such as sucrose, phenolic resins, furfural alcohol, acenaphthene and acetonitrile [19-22]. CMK-3 has been used as a support for various transition metals for carrying out a variety of catalytic transformations. Suzuki coupling by Pd/CMK-3, reduction of nitrobenzene and carbonyl compounds over Ru/CMK-3, hydrogenation of carbonyl compounds over Ni/CMK-3, oxidation of alcohols and conversion of amines to imines over FeO_x/CMK-3, aqueous phase reforming of glycerol and ethylene glycol over Pt/CMK-3, etc. have been reported [29-41]. Only scarce attempts such as base free oxidation of glucose to gluconic acid and catalytic reduction of p-nitrophenol into p-aminophenol were reported by using Au/CMK-3 [42, 43].

Herein we report the catalytic activity of Au/CMK-3 in the oxidative esterification of furfural. Furfural is a platform chemical from which number of medicines, pesticides, paints, plastics,

commodity chemicals and solvents etc. have been prepared [44]. At present the global production of furfural derivatives is at 947.58 kilo tons (2016) and the demand will grow at a compound annual growth rate (CAGR) of 2.69% to reach 1,172.17 kilo tons by 2024 [45]. Hence furfural is produced in large amounts from the biomass lignocellulose and such biomass is the subject of interest to many researchers [46]. Several fine chemicals such as furfural alcohol, 2-methyl furan, furoic acid, tetrahydrofuran (THF), cyclopentanol, cyclopentanone, 2-methyl tetrahydrofuran, polytetrahydrofuran, tetrahydrofurfuryl alcohol, etc. are also derived from furfural [47]. Recently furfural has been upgraded into gasoline and diesel fuels using efficient catalytic technologies [48]. One of the authors converted several biomasses into green fuels and the present authors have already reported the catalytic activities of Au-Pd/HAP-T and Au-Ag/HAP-T bimetallic catalysts towards the oxidative esterification of furfural [49-53]. The author performed this reaction using TBHP and air or O₂ at atmospheric pressure. However the present paper deals mainly with molecular O₂ or air at different pressures. Increase in pressure of O₂ increases the conversion and selectivity. Further the reaction was performed with O₂ at different pressures without using additional oxidants such as TBHP.

Any valorization process will be economically and environmentally attractive only when it is carried out under mild reaction conditions using non-corrosive reagents. Furfural can also be valorized into methyl 2-furoate which finds application in fine chemicals, flavor and fragrance industries [54]. As the conventional method of obtaining methyl 2-furoate uses strong oxidizing agent such as KMnO₄ and followed by esterification using concentrated sulphuric acid in methanol medium it causes harm to the environment. The other method of obtaining methyl 2-furoate also involves the strong bases such as NaOH, CH₃O⁻Na⁺, K₂CO₃, Li₂CO₃, CsCO₃ etc. but it is not an environmental benign method [55, 56]. Only scarce attempts have been made on the

oxidative esterification of furfural to methyl 2-furoate without using bases [57-62]. So herein we report the synthesis and characterization of Au/CMK-3 catalysts and the conversion of furfural to methyl 2-furoate with and without the use of various bases and oxidants (TBHP, air and O₂).

2. Experimental section

2.1 Materials

Tetraethylorthosilicate (TEOS, Merck), non-ionic triblock copolymers (P123, Poly(ethylene glycol)-block-poly(propylene glycol)-block-poly(ethylene glycol) (MW-5800); EO_nPO_mEO_n, Sigma Aldrich) and HCl (37%, Sigma Aldrich) were used for the synthesis of SBA-15.

Autoclavable PP bottles (Nalgene) were used for the hydrothermal preparation of SBA-15.

Glucose as a carbon source (SRL) and sulphuric acid (98%, Sigma Aldrich) as a catalyst were used for the preparation for CMK-3. Gold chloride (AuCl₃·3H₂O, 99.9%) purchased from Sigma Aldrich was used as a gold precursor. MWCNT (10 nm × 4.5 nm × 36 μm, Sigma Aldrich) and activated carbon (Alfa Aesar) were used as such. Graphite flakes were purchased (Natural-325 mesh, Alfa Aesar) and used for graphene synthesis. TiO₂ was synthesized by sol-gel method from titanium-isopropoxide (Sigma Aldrich).

2.2 Synthesis of mesoporous SBA-15 via hydrothermal method

Mesoporous silica SBA-15 with gel composition 1 TEOS: 5.87 HCl: 194 H₂O: 0.017 P123 was synthesized using the silicon source tetraethylorthosilicate (TEOS) and structure directing agent Pluronic P123 in a highly acidic medium [7]. In a PP bottle, 4 g of triblock-copolymer, 130 ml of water and 20 ml of concentrated HCl were added and stirred for 2 h for complete dissolution and the temperature was maintained at 318 K. The silica source tetra ethylorthosilicate (TEOS) was then added directly to the above solution with constant stirring maintaining the above

temperature for 24 h. The white suspension resulting was autoclaved at 318 K in an air oven for 24 h and cooled. The resultant white suspension was centrifuged, washed with water and dried at 393 K for 12 h. The white material formed was ground and calcined at 823 K for 6 h for the complete removal of the templates and to obtain mesoporous SBA-15 material.

2.3 Synthesis of mesoporous CMK-3 carbon via nanocasting method

In the typical synthesis of mesoporous CMK-3, SBA-15 was used as a hard template. In order to ensure complete polymerization and carbonization, sucrose coatings were done twice as reported by us [63, 64]. To 1 g of the SBA-15 material, 1.25 g of sucrose, 0.1 g of concentrated H₂SO₄ and 5 ml of deionised H₂O were added and stirred until thick slurry was formed. Then it was dried in an air oven at 383 K for 6 h and carbonized at 433 K for another 6 h. The obtained brown material was finely ground and used for the second coating of the sucrose precursor. To the above brown mixture, 0.8 g of sucrose, 0.08 g of conc.H₂SO₄ and 5 ml of deionised H₂O were added, and the same procedure was repeated. The black mass obtained was ground and finally carbonized at 1173 K for 6 h under the flow of N₂. The carbonized material was then stirred with 5% HF solution for 12 h and washed with ethanol to obtain the nanoporous carbon CMK-3.

2.4 Synthesis of mesoporous Au/CMK-3 catalysts via high temperature H₂ reduction

In the typical synthesis, 1 g of CMK-3 was dispersed in 20 ml of acetone and stirred for 5 min. Then yellow colored HAuCl₃ solution (0.05 mM) was added and stirred for 2 h. A transparent solution obtained indicates that the Au³⁺ ions were adsorbed onto the nanoporous carbon. The resulting solution was dried at 383 K and reduced under the flow of hydrogen (30 ml/min) at

673 K for 3 h to get 1 % Au/CMK-3 (w/w) nanocatalyst. Similarly by varying the amount of gold stock solution, 3%, 5% and 7 % of Au/CMK-3 (w/w) nanocatalysts were obtained.

2.5 Synthesis of other catalysts

Graphite oxide (GO) was synthesized from graphite powder via modified Hummer's method and the method reported by us earlier [65]. Then it was ground, dispersed in ethanol and sonicated for 30 min. To this, gold precursor was added and sonicated for another 15 min. For drying, calcination and reduction the procedure described for CMK-3 was adopted. Nano titanium dioxide (TiO₂) was synthesized using sol-gel method as reported by us earlier [66]. MWCNT and activated carbon were used as such without any modification. All these materials were impregnated with 5% Au by following the same procedure given in Section 2.4.

2.6 Characterization of catalysts

X-ray powder diffraction patterns of Au/CMK-3 were recorded using a Philips X-Pert diffractometer equipped with a Ni β filter and Cu K α radiation with $\lambda=1.5406 \text{ \AA}$ working at the operating voltage of 40 kV and the current of 30 mA. Low angle data were collected in the 2θ range from 0.6 to 10 at a scan size of 0.01° at a scan time of 10 s. The wide angle data were collected in the 2θ range from 10 to 80 at a scan size of 0.04° . Peak identification was performed with Origin 8 software. The standard reference for metallic Au was obtained from the JCPDS database. The average particle size was calculated in a direction perpendicular to the crystallographic plane based on Scherrer formula by equation 1:

$$X_s = \frac{0.9 \times \lambda}{\beta \times \cos\theta} \quad (1)$$

Where, λ – is the wavelength of the monochromatic X-ray beam (Cu-K $_{\alpha 1}$, 1.54056 Å°); β_{hkl} – broadening of the hkl diffraction peak measured at half of its maximum intensity (radians) and θ – diffraction angle [67].

Nitrogen adsorption - desorption isotherms were constructed at 77 K using a constant volume adsorption apparatus (Micrometrics ASAP 2020) for the determination of surface area and other texture characteristics. Prior to the analysis, CMK-3 samples were degassed and pretreated at 583 K for 6 h. The specific surface area was calculated from the Brunauer –Emmett – Teller (BET) equation from the adsorption data in the relative partial pressure from 0.05 to 0.3. The total pore volume was derived from the BET plot by calculating the amount of N₂ at a partial pressure of 0.95. The pore size distribution (PSD) was calculated from the desorption branch of the isotherm using Barrett – Joyner – Halenda (BJH) model.

Catalyst morphology and structure of Au/CMK-3 were studied using Quanta 200 FEG scanning electron microscope (HR-SEM) and the composition analysis was performed using energy-dispersive X-ray spectroscopy (EDS). Prior to the analysis, powdered samples were dried at 373 K for 6 h, air dispersed over the carbon tape and mounted for analysis. The high resolution transmission electron micrographs (HR-TEM) were recorded using JEOL JEM-2100JF working at the operating voltage of 200 keV. Powder samples were dispersed in absolute ethanol, ultrasonicated for 10 minutes, placed over holey carbon coated Cu grid, dried at ambient conditions and mounted for the analysis.

Quantitative determination of gold was carried out by inductively coupled plasma (ICP) technique using Perkin Elmer Optima 5300 DV. 200 mg of samples were digested in mixture of concentrated acid for 6 h, diluted and filtered through syringe filter prior to the analysis.

XPS measurements were carried out to find out the elements present in the mesoporous catalysts on an ESCA+, Omicron Nanotechnology ESCA Probe spectrometer with monochromatized AlK_{α} X-rays (energy: 1486.6 eV) 300W with base pressure of 5×10^{-5} mB. Sputter-cleaned $Cu_{2p_{3/2}}$ (932.7 eV) and $Au_{4f_{7/2}}$ (84.0 eV) core level peaks (from foils) were used to calibrate the XPS instrument. The catalyst samples were pelletized, dried at 398 K under vacuum and mounted in the sample port. Spectra in the required binding energy range were collected for 8 times (except survey scan) and an average spectrum was taken. The binding energy (B.E) scale was referenced by setting the C (1s) binding energy (B.E) of adventitious carbon to 284.6 eV. XPS high-resolution scans were performed for the $Au_{4f_{5/2}}$, $Au_{4f_{7/2}}$ and C1s.

2.7 Catalytic experiments

The liquid phase oxidative esterification of furfural in the methanol medium using different oxidants such as tert-butyl hydroperoxide (TBHP) was investigated using a batch reactor of 150 ml capacity made up of glass at 393 K as reported by us [53]. 0.3ml of furfural, 3 eq. of TBHP (70%) and 50 mg of catalyst were added to 20 ml of methanol and the reaction was performed in liquid phase. Thin layer chromatography (TLC) was used to study the progress of the reaction using petroleum ether: ethyl acetate (9:1) as mobile phase. After the reaction, catalyst was separated by centrifuging and then treated with chloroform water mixture in a separating funnel for the removal of excess of methanol. The golden yellow layer was separated and dried over anhydrous sodium sulphate. Air or O_2 were fed into the high pressure reactor made up of stainless steel with 100 ml capacity [Parker autoclaves engineers]. After 3 h of reaction, the reactor was allowed to cool in cold water and the sample aliquots (30 μ L) was centrifuged, filtered through nylon syringe filters (0.22 microns) and analyzed using gas chromatograph

(Shimadzu GC-17A) equipped with a ZB-FFAP capillary column and a flame ionization detector (FID).

3. Results and discussion

3.1 Powder X-ray diffraction

The low angle x-ray powder diffraction patterns of SBA-15 and CMK-3 were recorded to determine the structural order. Fig.S1 shows the low angle x-ray powder diffraction of mesoporous silicious SBA-15 and its carbon replica phase CMK-3. The texture parameters are given in Table.1.

Figure.S1

Both SBA-15 and CMK-3 show strong reflections in the low angle indicating the uniform pore structures. The powder diffraction patterns of silicious SBA-15 show sharp peak at $2\theta = 0.96$ (100) and two weak reflections at the angles of $2\theta = 1.62$ (110) and 1.84 (200). Similarly CMK-3 obtained from the replica of SBA-15 also shows a sharp and well intense peak at $2\theta = 1.03$ (100) and the weak peaks at 1.77 (110), 2.06 (200) [68-70]. SBA-15 material possesses 2D hexagonal mesoporous structure with long range order connecting micropores and small mesopores [71]. As the replica CMK-3 was obtained from the pore filling of SBA-15, uniform sized hexagonal carbon rods with interlinked carbon bridges were formed. This is indexed in the hexagonal lattice with the crystallographic space group of $p6mm$ [72].

The XRD peaks of CMK-3 were found to be broader, less intense and observed at slight by higher 2θ angle than SBA-15. The periodic distance decreases when CMK-3 shrinks and distorts at high temperature treatments and hence there is slight broadening and slight shift in the

diffraction angles. Such deformations in the periodic structures are frequently observed in the synthesis of mesoporous carbon. The d_{100} for SBA-15 and CMK-3 were found to be 9.2 nm and 8.6 nm. The corresponding unit cell parameters calculated using the formula $a_0=2d_{100}/\sqrt{3}$ were 10.6 nm and 9.9 nm respectively. The unit cell parameter (a_0) of CMK-3 decreases in comparison with SBA-15 indicates the structural shrinkage due to nanocasting. These calculated d spacing and unit cell parameters are in good agreement with the reported literature [73, 74].

Fig.1 depicts the low angle x-ray powder diffraction patterns of 1%, 3%, 5% and 7% Au/CMK-3 catalysts. All the catalysts show sharp, intense peak around $2\theta = 1.03$ (100) and two less intense peaks at $2\theta = 1.77$ (110) and $2\theta = 2.05$ (200). The introduction of Au into the mesopores of the CMK-3 generally increase the scattering effect which further increase the phase cancellation between scattering from the walls and pores. Due to this reason, the increase in Au content from 1% to 7%, further decreased the peak intensity [75, 76]. The XRD patterns of Au impregnated CMK-3 catalysts reveal that the structural periodicity is not lost despite the introduction of Au and higher calcination/reduction temperature employed during the synthesis.

Figure.1

Fig.2 presents the wide angle x-ray diffraction patterns of Au/CMK-3 with different Au (1 %, 3 %, 5 % and 7 %) contents and compared with the JCPDS pattern of pure metallic Au.

Figure.2

The effect of dispersion and crystalline nature Au metal nano particles over CMK-3 is better observed from the wide angle diffraction pattern. Only 5% Au/CMK-3 and 7 % Au/CMK-3 catalysts show weak characteristic peak for Au (FCC lattice) at $2\theta = 38.2$ (111) indicating the formation of Au nano clusters outside the mesochannels of CMK-3 [77]. However Au (1% &

3%)/ CMK-3 catalysts, the peaks corresponding to Au at $2\theta = 38.24(111)$, $44.32(200)$, $64.4(220)$ are not observed due to the fact that Au nano particles are dispersed within the mesochannels. However when the concentration of Au increased to 5% or 7%, less intense diffraction peaks were observed owing to the dispersion of Au nano particles on the surface. Similar such reports have been reported for Pt/CMK-3 [78]. The average particle size was calculated to be 2.3 nm and 2.5 nm for 5% and 7% respectively. Further texture evidence of Au nano structures over CMK-3 is detailed with N₂ adsorption studies.

3.2 Nitrogen sorption analysis

The texture characteristics of porous materials through N₂ adsorption at low temperature (77 K) provide information about the microporosity and mesoporosity. Adsorption – desorption isotherm exhibit a hysteresis loop provides information about the shape and size of the mesopores [79]. The N₂ adsorption - desorption isotherm and the pore size distribution of SBA-15 and CMK-3 are shown in Figs. S2 and S3.

Figure. S2

Figure. S3

Both SBA-15 and CMK-3 materials exhibit typical type IV isotherm with H₁ hysteresis loop (0.6 - 0.8) which is characteristic of capillary condensation in the mesochannels according to the IUPAC classification. A sharp increase at lower P/P_o (0.45) indicates that the pores are expected to be narrow [80, 81]. Surface area, pore volume, pore diameter and carbon wall thickness calculated for SBA-15, CMK-3 and Au/CMK-3 (1%, 3%, 5% and 7 %) are summarized in Table.1.

Table.1

It is evident from the texture properties that CMK-3 derived from the SBA-15 as template shows the highest surface area of 1096 m²/g followed by SBA-15 of 740 m²/g. These values are in good agreement with literature reports [82]. This difference may be due to the bulk density difference between carbon (1.8 ml/g) and silica (2.2 ml/g) [83]. The decreased pore diameter and pore volume of CMK-3 when compared to SBA-15 may be due to the increased microporosity in the nano channels. The pore size distribution (PSD) of SBA-15 and CMK-3 calculated from the BJH model were 7.69 nm and 4.56 nm respectively and the peak was found to be sharp which is indicative of uniform regular pores. The N₂ adsorption - desorption isotherms and the pore size distribution (PSD) of Au/CMK-3 with different Au contents (1%, 3%, 5% and 7 %) are illustrated in Fig.S4 and S5 respectively.

Figure. S4**Figure. S5**

All the Au/CMK-3 catalysts show similar type IV isotherm with H₁ hysteresis loop which is typical for mesoporous materials. Surface area (S_{BET}) decreased from 1039 m²/g to 880 m²/g as the content of Au increased from 1% to 7 %. The pore volume and pore diameter also gradually decreased with increase in Au content. The pore volume decreased from 0.97 cm³/g to 0.81 cm³/g, the pore diameter decreased from 4.10 nm to 3.80 nm and the wall thickness increased from 5.99 nm to 6.09 nm. In general, type, size and shape of the metal, preparation methods and the amount of loading are the important factors which are responsible for either decrease or increase in the texture properties [84-89].

3.4 X-ray photoelectron spectroscopy (XPS)

X-ray photoelectron spectral analysis were further performed on CMK-3, 3% Au/CMK-3, 5% Au/CMK-3 and 7% Au/CMK-3 and the corresponding XPS survey spectra are shown in Fig. S6.

Figure. S6

The survey spectrum of CMK-3 shows core levels of C1s (284.7 eV) and O1s (529.5 eV) after the charge correction. Au peaks at 83.37 eV and 97.03 eV are noticed due to the core levels of Au 4f_{7/2} and Au 4f_{5/2}. These values are in good agreement with the reported ones [90, 91].

Fig. 3 shows the XPS core level spectra of 1%, 3%, 5% and 7% Au/CMK-3.

Figure.3

Among the Au loaded catalysts, only 5% Au/CMK-3 and 7% Au/CMK-3 catalysts show corresponding core level peaks for Au at 83.37 eV (Au 4f_{7/2}) and 87.03 eV (Au 4f_{5/2}). 1% Au/CMK-3 and 3% Au/CMK-3 did not show any core level peaks for Au due to the presence of Au particles within the pores making inaccessible for the analysis.

Table.1 shows the Au metal content values determined by various instrumental techniques such as ICP, EDS and XPS. The Au metal concentration determined by EDS and XPS in 5% and 7% Au/CMK-3 catalysts were found to be lower when compared with the values obtained from the ICP results. This clearly shows that most of the Au particles are retained in the pores. The Au diffraction peaks found only in 5% Au/CMK-3 and 7% Au/CMK-3 catalysts in their XRD analysis further support this observation.

3.5 High resolution scanning electron microscope (HR-SEM)

The morphological structure of SBA-15 and CMK-3 was investigated by high resolution scanning electron microscope (HR-SEM) in Fig.4 (a-d). Low magnified HR-SEM images of SBA-15 show uniform and linear rod like morphology arranged together to form bundles as shown in Fig.4 (a). Similarly CMK-3 obtained from SBA-15 also shows similar lengthy rod like morphology with similar dimensions of 20 micron x 400 nm as shown in Fig.4 (b). These images clearly show the successful replication process of SBA-15. In the high magnification image of CMK-3 it is noticed that the width of the bundle decreased (Figs.4 (b) and 4 (d)). This may be due to the shrinkage occurred during the high temperature treatment. The obtained micrographs of SBA-15 and CMK-3 are in good agreement with the previous literature reports [92].

Figure.4

On high magnification, the HR-SEM of SBA-15 shows rods of width ≈ 380 nm whereas the CMK-3 rods show rods of ≈ 333 nm but importantly without much irregular carbon deposits. This study reveals that just enough quantity of sucrose has been used in the replication process. It is evident that the individual rods of CMK-3 are arranged in an array forming long bundles of structure. The HR-SEM of the representative samples of Au loaded CMK-3 are shown in Fig.5 (a-b). Gold particles are not seen in the HR-SEM but clearly seen in the HR-TEM (discussed later). The highly magnified micrographs of Au/CMK-3 with 5% and 7% Au show similar surface structure indicating that Au has been incorporated into the channels of CMK-3 matrix as shown in Fig. 5 (c).

Figure.5

However during the impregnation of gold chloride over CMK-3, the yellow colour of the precursor becomes transparent indicating that the gold ions are adsorbed completely by CMK-3. The effect of strong capillary force within the pore channels with high specific surface area and high adsorption capacity of CMK-3 makes the precursor Au^{3+} to be highly adsorbed into the channels during the impregnation process. This material which on reduction under H_2 atmosphere yields highly dispersed Au nano structures. Even at high loading of Au at 7 % the gold nano structures are too small to be identified by HR-SEM. However the EDS analysis of 5% Au/CMK-3 shows a very small peak at the binding energy of 2.120 KeV as shown in Fig.5 (d). Similar weak peak was also obtained in the XRD patterns at $2\theta = 38.2$ (111). However the presence of the Au nano particles is better seen from the HR-TEM micrographs.

3.6 High resolution transmission electron microscope (HR-TEM)

The morphology of the silica template SBA-15 and the carbon replica CMK-3 support were also examined by HR-TEM technique and the micrographs are shown in Fig.S7 (a & b).

Figure.S7

The periodic, structural and texture properties of both SBA-15 and the carbon replica CMK-3 are similar. These images suggest that even after the replication process and high temperature reduction the structure of CMK-3 remains intact. The sizes of SBA-15 and CMK-3 rods measured from the HR-TEM analysis were found to be 360 nm and 300 nm respectively. These are in agreement with the HR-SEM values.

The structure and extent of Au dispersion over CMK-3 are also examined by HR-TEM technique. The HR-TEM micrographs of 5% and 7 % Au/CMK-3 catalysts are shown in Fig. 6 (a-f). Low magnification images of Au loaded CMK-3 show comparable structure and no gold

particles are seen in these images (Fig. 6 (a) & (b)). However, high magnification images of 5% Au/CMK-3 and 7% Au/CMK-3 catalysts show Au nano particles dispersed nicely without any agglomeration as shown Fig. 6 (c) & (d).

Figure.6

60 particles were chosen from HR-TEM micrograph of 5% Au/CMK-3 to find out the average particle size distribution and they were found to be in the narrow range of approximately 1- 4 nm with maximum particles around 2.5 nm (Fig.6e). The determined values are in good agreement with the average particle size calculated using Scherrer equations from the high angle XRD diffraction pattern. The lattice fringe was determined to be $d = 0.2380$ nm for the corresponding metallic Au.

3.7 Catalytic studies on oxidative esterification of furfural

3.7.1 Evaluation of catalytic activities of various supported catalysts: The oxidative esterification of furfural to methyl 2-furoate(as shown in Scheme.1) was carried out in a batch reactor using methanol as solvent, TBHP as an oxidant over various Au supported catalysts such as Au/CMK-3, Pd/CMK-3, Pt/CMK-3 and Ni/CMK-3, Au/SBA-15, Au/graphite, Au/graphene, Au/MWCNT, Au/activated carbon, Au/TiO₂ and the results are given in Table.2.

Table.2

Among the Au supported catalysts Au/TiO₂ showed maximum conversion of furfural (93.9%) followed by Pd/CMK-3, Au/CMK-3, Au/graphite etc. But Au/TiO₂ showed poor selectivity towards the desired product of methyl 2-furoate. Although Ni/CMK-3 shows 100% selectivity towards methyl 2-furoate, it is able to convert only 29.1% of furfural. As far as

Au/CMK-3 is concerned, it gives the best conversion of furfural (77.7 %) and selectivity towards methyl 2-furoate (96.8%). The superior activity of CMK-3 support over other supports is evident from the above results. This may be due to the very good dispersion of smaller Au particles onto the pore channels of CMK-3. Further, the oxidative esterification does not produce any alkyl peroxides.

3.7.2 Optimization of reaction conditions

3.7.2.1 Optimization of Au content: The effect of Au content on the catalytic oxidative esterification of furfural was studied by varying the Au content from 1 % to 7 % at the same reaction conditions and the results are given in Table.3.

Table.3

Although there is not much difference in % selectivity of methyl 2-furoate, a significant difference in % conversion was observed over 1, 3, 5 % Au/CMK-3 catalysts. However on increasing the Au content further to 7% there was no remarkable improvement in both the % conversion and % selectivity. Higher loading of 7% Au impregnation over CMK-3 induces agglomeration and may result in a slight loss of catalytic activity. The HR-TEM images of these two catalysts also suggest the higher agglomeration of Au on 7% Au/CMK-3 than on 5% Au/CMK-3. Hence 5% Au/CMK-3 has been chosen for further optimization studies.

3.7.2.2 Effect of reaction temperature on the catalytic activity: The effect of reaction temperature on the conversion of furfural and the selectivity towards methyl 2-furoate was investigated in the temperature range of 333 K to 413 K over 5% Au /CMK-3 catalyst under the same reaction conditions and the results obtained after 3 h are given in Table.4.

Table.4

The results clearly show that the reaction temperature plays a definite role in the conversion of furfural as only 23.5% of furfural was converted at 333 K and it increases as high as 77.7% with increase in temperature (393 K). Increasing reaction temperature also decreases the selectivity towards methyl 2-furoate due to the formation of 4-furaldehyde-dimethyl-acetal. Hence 393 K was found to be the optimum temperature. The effect of time on stream on the catalytic activity was also studied for 5 h at the reaction temperature of 393 K and the results are given in Table.5.

Table.5

Table.5 indicates that conversion increased with time and reached maximum of 85.1 % at the 5th hr. However the selectivity to methyl 2-furoate decreased with time on stream. Hence reaction time has been optimized at 3 h.

3.7.2.3 Effect of various bases on the catalytic activity:

In general such oxidative esterification of furfural is carried out by using various bases such as NaOH, NaOCH₃, K₂CO₃, Li₂CO₃ and CsCO₃. Hence in order to check the influence of the base on the conversion and selectivity, 5 ml of 10% aqueous solution of bases was added and the reaction was performed in O₂ atmosphere under the optimized conditions but without TBHP and the results are given in Table.6.

Table.6

It was found that bases also convert furfural with reasonable conversion and selectivity towards methyl 2-furoate. Among the various bases, the order of catalytic reactivity was found to be

$\text{CsCO}_3 > \text{Li}_2\text{CO}_3 > \text{NaOCH}_3 > \text{K}_2\text{CO}_3 > \text{NaOH}$. As the bases are corrosive in nature and not environmentally benign they are to be avoided for such conversions.

3.7.2.4 Effect of oxidants on the catalytic activity: In the present study different oxidants such as tert-butyl hydroperoxide, air and oxygen have been used for the oxidative esterification of furfural. The reaction was performed under the optimized reaction conditions over 5% Au/CMK-3 and the results obtained are given in Table.7.

Table.7

Air at ambient conditions does not convert furfural and the conversion increased with increasing pressure of air and oxygen. However reactions carried out under the optimized reaction temperature in air and oxygen at high pressure (5-15 bar) shows increased conversion and selectivity. With the increase in the operating pressure from 0 to 15 bar with air and oxygen, the conversion of furfural and selectivity to methyl 2-furoate increases. The reaction carried out in presence of oxygen at 15 bar shows higher conversion of furfural (99.7%) and higher selectivity (99.6%) than air atm. The selectivity towards the undesired product namely 4-furaldehyde dimethyl- acetal was found to be in the range of 3.2 % to 9.9%, however when air or oxygen alone was used the selectivity towards this undesired product was found to be less than 1. Hence this study clearly indicates that for both selectivity and economic points of view, the oxidative esterification of furfural can be done effectively by using only oxidants such as air and oxygen.

3.7.2.5 Effect of reusability of 5% Au/CMK-3 catalyst:

In order to investigate the reusability of the 5% Au/CMK-3 catalyst, the oxidative esterification of furfural was carried out successively for another five times at 393 K in O₂ atmosphere (15 bar). The catalysts after 3 h of reaction time was gently washed with water and methanol and reused. The efficiency was investigated for five catalytic cycles and the results are given in Table.8.

Table.8

The conversion and selectivity results reveal that 5% Au/CMK-3 catalyst is a sturdy catalyst and can be reused without much loss of catalytic activity. Au/CMK-3 prepared by Qi et. al. (2015) showed loss of catalytic activity from 92% to 70% in the base free oxidation of glucose to gluconic acid after 4 catalytic cycles [42]. The authors have impregnated Au over CMK-3 in the aqueous medium followed by sodium borohydride reduction. Since the CMK-3 material is highly hydrophobic in nature, the CMK-3 will prefer the Au particle to occupy the surface and not into the pores and hence there was a loss in the catalytic activity due to leaching. Moreover the particle will have bigger size. However our method of synthesis of Au/CMK-3 involves the deposition of Au in organic medium followed by hydrogen reduction. This method has the advantage of keeping the Au particles inside the pores of CMK-3 and hence the Au particles are not leached during the reaction. Similar observations were made by Ryoo. et. al. (2001) over Pt clusters over CMK-3[92]. The particle inside the pores has the pore size distribution in the range of 1-3 nm. Therefore the catalytic activity is retained even after five cycles. This study also clearly indicates the importance of method of preparation of catalysts. Figure.7 shows the HR-TEM micrographs and the average particle size distribution of the spent catalyst used for five catalytic cycles. The intact nature of the Au particles with no aggregation was noticed.

Figure.7

In order to check the effect of oxidants such as TBHP and oxygen on metal leaching, catalysts after five catalytic cycles were subjected to ICP analysis to know the Au concentration. Prior to analysis the catalysts were washed with distilled water, methanol, dried at 393 K and digested in a mixture of concentrated acids. The Au content in the spent catalyst (5% Au/CMK-3) catalyzed in the O₂ atmosphere was found to 4.82% which is much closer to the theoretical value of 5%. But when the Au content in the spent catalyst (5% Au/CMK-3) catalyzed along with TBHP was found to be 4.32% showing much loss due to leaching in the reaction. Thus it is concluded that the hydrophobicity keeps the Au metal particles onto the pores of CMK-3 helping in well dispersion of Au particles in the size range of 1-3 nm without agglomeration.

Moreover, the usage of TBHP as an oxidant introduces new functional groups such as –OH, –COOH etc, on the surface of CMK-3. Fig.8 shows the FT-IR spectra of the spent catalyst (5% Au/CMK-3) catalyzed along with TBHP at two different reaction temperatures (393 K & 413 K) showed OH stretching peak at 3438 cm⁻¹, the C=O stretching peaks at 1720 and 1563 cm⁻¹, the C-O-C bending vibration at 1233 cm⁻¹. Slightly higher leaching of Au particles was noticed in the spent catalyst used along with TBHP. This is because of creation of the above mentioned functional groups, opening up a thin layer of surface leading to slight leaching of the Au particles. The presence of functional groups is also responsible for the formation of undesired products namely 4-furaldehyde dimethyl-acetal.

Figure.8**4. Conclusions**

CMK-3 was successfully synthesized using a hard template SBA-15, and sucrose, a carbon source, using nanocasting method. Au was impregnated over different supports such as SBA-15, graphite, graphene, MWCNT, activated carbon and TiO₂ and their catalytic activities were compared. Among the catalysts 5% Au/CMK-3 was found to be the best catalyst in terms of conversion (99.7%) and selectivity (99.6 %) under the O₂ pressure of 15 bar. Various Au/CMK-3 catalysts with different Au contents were prepared using wet impregnation method followed by hydrogen reduction. The XRD and BET analysis confirm the mesostructure of the catalyst while the HR-SEM and HR-TEM micrographs confirm the rod like morphology for both CMK-3 and Au/CMK-3 catalysts. Fine dispersion of Au particles over CMK-3 was evidenced by HR-TEM. The study of effect of metal ion on the catalytic activity shows that Au catalysts are the best catalysts in terms of furfural conversion and selectivity towards methyl 2-furoate. Similarly, the study on the effect of support on the catalytic activity shows that CMK-3 is the best support. Optimization studies revealed that the reaction temperature of 393 K and the reaction time of 3 h yield maximum conversion of furfural and selectivity towards methyl 2-furoate. The study on effect of oxidants on the catalytic activity indicated that among the different oxidants namely TBHP, O₂ and air, O₂ was found to be the best oxidant as it offers very high catalytic activity. Unlike TBHP the oxidative esterification of furfural in presence of oxygen does not create any unwanted functional groups on the surface of the catalysts and hence improves the selectivity. Among the Au/CMK-3 catalysts, 5% Au/CMK-3 was found to be the most active catalyst as it converted 99.7% of furfural with methyl 2-furoate selectivity as high as 99.6%. The recyclability of 5% Au/CMK-3 proved that the catalyst did not show much loss in the catalytic activity even after five catalytic cycles.

Acknowledgement

The authors acknowledge the funding received from DRDO-LSRB and CPRI, INDIA.

References

- [1] A. Corma, *Chem. Rev.*, 97 (1997) 2373- 2420.
- [2] M. Moritz and M. G. Moritz, *Mater. Sci. Eng., C*, 49 (2015) 114–151.
- [3] N. Linares, A. M. S. Albero, E. Serrano, J. S. Albero and J. G. Martinez, *Chem. Soc. Rev.*, 43 (2014) 7681-7717.
- [4] Vallet-Regi, Balas F and Arcos D., *Angew Chem Int Ed Engl.*, 46/40 (2007) 7548-7558.
- [5] C. T. Kresge, M. E. Leonowicz, W. J. Roth, J. C. Vartuli and J. S. Beck, *Nature*, 359 (1992) 710 - 712.
- [6] T. Yanagisawa, T. Shimizu, K. Kuroda and C. Kato, *Bulletin Bull. Chem. Soc. Jpn*, 63 (1990) 988-992.
- [7] D. Zhao, J. Feng, Q. Huo, N. Melosh, G. H. Fredrickson, B. F. Chmelka and G. D. Stucky, *Science*, 279 (1998) 548-552.
- [8] V. Meynen, P. Cool and E. F. Vansant, *Microporous Mesoporous Mater.*, 125 (2009) 170–223.
- [9] Y. Wan and D. Zhao, *Chem. Rev.*, 107 (2007) 2821-2860.
- [10] D. Zhao, Q. Huo, B. F. Chmelka and G. D. Stucky, *J. Am. Chem. Soc.*, 120 (1998) 6024-6036.
- [11] R. Ryoo, S. H. Joo , and S. Jun, *J. Phys. Chem. B*, 103/37 (1999) 7743–7746.
- [12]. S. H. Joo, S. Jun and R. Ryoo, *Microporous Mesoporous Mater.*, 44–45 (2001) 153–158.

- [13] R. Ryoo, S. H. Joo, M. Kruk and M. Jaroniec, *Adv. Mater.*, 13 (2001) 671-681.
- [14] A. H. Lu and F. Schuth, *Adv. Mater.*, 18 (2006) 1793-1805.
- [15] T. Ohkubo, J. Miyawaki, K. Kaneko, R. Ryoo and N. A. Seaton, *J. Phys. Chem. B*, 106 (2002) 6523-6528.
- [16] Y. Sakamoto, M. Kaneda, O. Terasaki, D. Zhao, J.M. Kim, G. D. Stucky, H. J. Shin and R. Ryoo, *Nature*, 408 (2000) 449-453.
- [17] S. Jun, S. H. Joo, R. Ryoo, M. Kruk, M. Jaroniec, Z. Liu, T. Ohsuna and O. Terasaki, *J. Am. Chem. Soc.*, 122 (2000) 10712-10713.
- [18] P. Niebrzydowska, R. Janus, P. Kuśtrowski, S. Jarczewski, A. Wach, A. M. Silvestre-Albero and F. R. Reinoso, *Carbon*, 64 (2013) 252-261.
- [19] H. J. Shin, R. Ryoo, M. Kruk, M. Jaroniec, *Chem. Commun.*, (2001)349-350.
- [20] H. Darmstadt, C. Roy, S. Kaliaguine, S. J. Choi and R. Ryoo, *Carbon*, 40 (2002) 2673-2683.
- [21] M. Kaneda, T. Tsubakiyama, A. Carlsson, Y. Sakamoto, T. Ohsuna and O. Terasaki, *J. Phys. Chem. B*, 106 (2002) 1256-1266.
- [22] S. H. Joo, S. J. Choi, I. Oh, J. Kwak, Z. Liu, O. Terasaki and R. Ryoo, *Nature*, 412 (2001) 169-171.
- [23] T. W. Kim, R. Ryoo, K. P. Gierszal, M. Jaroniec, L. A. Solovyov, Y. Sakamoto and O. Terasaki, *J. Mater. Chem.*, 15 (2005) 1560-1571.

- [24] T. Maiyalagan, Abu Bakr A. Nassr, T.O. Alaje, M. Bron and K. Scott, *J. Power Sources*, 211 (2012) 147–153.
- [25] C. Yu, J. Fan, B. Tian, D. Zhao and G. D. Stucky, *Adv. Mater.*, 14 (2002) 1742-1745.
- [26] T. W. Kim, R. Ryoo, K. P. Gierszal, M. Jaroniec, L. A. Solovyov, Y. Sakamoto and O. Terasaki, *J. Mater. Chem.*, 15 (2005) 1560–1571
- [27] T. W. Kim, I. S. Park, and R. Ryoo, *Angew. Chem. Int. Ed.*, 42 (2003) 4375 –4379.
- [28] J. Lee, S. Yoon, T. Hyeon, S. M. Oh and K. B. Kim, *Chem. Commun.*, 1999, 2177-2178.
- [29] H. Huang, X. Wang, M. Tan, C. Chen, X. Zou, W. Ding and X. Lu, *Chem. Cat. Chem.*, 8 (2016) 1485-1489.
- [30] H. R. Choi, S. Jang, J. Y. Cheon, C. Kim, J. Park, K. H. Park and S. H. Joo, *Chem. Cat. Chem.*, 4 (2012) 1587-1594.
- [31] J. Hu, Y. Ding, H. Zhang, P. Wu and X. Li, *RSC Adv.*, 6 (2016) 3235-3242.
- [32] Y. Ding, X. Li, H. Pan and P. Wu, *Catal. Lett.*, 144 (2014) 268-277.
- [33] Y. Ding, X. Li, B. Li, H. Wang and P. Wu, *Catal. Commun.*, 28(2012) 147–151.
- [34] D. Kim, H. Kang, H. Park, S. Park, J. C. Park and K. H. Park, *Eur. J. Inorg. Chem.*, 21(2016) 3469-3473.
- [35] L. Geng, J. Song, B. Zheng, S. Wu, W. Zhang, M. Jia and G. Liu, *Chinese J. Catal.*, 37 (2016) 1451–1460.

- [36] H. Qiao, J. Li, J. Fu, D. Kumar, Q. Wei, Y. Cai, and F. Huang, *ACS Appl. Mater. Interfaces*, 3(2011) 3704–3708.
- [37] V. Celorrio, D. Sebastian, L. Calvillo, A.B. García, D.J. Fermin and M.J. Lazaro, *Int. J. Hydrogen Energy*, 41 (2016) 19570–19578.
- [38] T. W. Kim, H. D. Kim, K. E. Jeong, H. J. Chae, S. Y. Jeong, C. H. Lee and C. U. Kim, *Green Chem.*, 13 (2011) 1718-1728.
- [39] V. Ravat, I. Nongwe and N.J. Coville, *Microporous Mesoporous Mater.*, 225 (2016) 224–231.
- [40] V. Valles, B. Ledesma, J. Juarez, M. G. Costa, O. Anunziata and A. Beltramone, *Fuel*, 188 (2017) 155–165.
- [41] M. Oschatz, T. W. van Deelen, J. L. Weber, W. S. Lamme, G. Wang, B. Goderis, O. Verkinderen, A. I. Dugulanc and K. P. de Jong, *Catal. Sci. Technol.*, 6 (2016) 8464-8473.
- [42] P. Qi, S. Chen, J. Chen, J. Zheng, X. Zheng, and Y. Yuan, *ACS Catal.*, 5 (2015) 2659–2670.
- [43] P. Guo, L. Tang, J. Tang, G. Zeng, B. Huang, H. Dong, Y. Zhang, Y. Zhou, Y. Deng, L. Ma and S. Tan, *J. Colloid Interface Sci.*, 469 (2016) 78–85.
- [44] R. Mariscal, P. Maireles Torres, M. Ojeda, I. Sadabaa and M. Lopez Granados, *Energy Environ. Sci.*, 2016, DOI: 10.1039/C5EE02666K.
- [45] *Furfural Derivatives Market - Global Industry Analysis, Size, Share, Growth Trends, and Forecast 2016 – 2024*, Transparency Market Research, 2016.

- [46] K. J. Zeitsch, *The Chemistry and Technology of Furfural and its many by-products*, Elsevier, Amsterdam, 2000.
- [47] Furkan H. Isikgor and C. Remzi Becer, *Polym. Chem.*, 6 (2015) 4497-4559.
- [48] Jean-Paul Lange, Evert van der Heide, Jeroen van Buijtenen and Richard Price, *ChemSusChem*, 5 (2012) 150 – 166.
- [49] G. Ramya, R. Sudhakar, J. Amala Infant Joice, R. Ramakrishnan and T. Sivakumar, *Appl. Catal. A: General*, 8 (2012) 170-178.
- [50] G. Ramya, R. Sudhakar, K. Kathiravan and T. Sivakumar, *Adv. Porous Mater.*, 2 (2014) 113-123(11).
- [51] G. Ramya, T. Sivakumar, M. Arif and Z. Ahmed, *Energy sourc. A, Recovery util. environ. effects*, 37 (2015) 878 - 885.
- [52] G. Ramya, T. Sivakumar, M. Arif and Z. Ahmed, *Energy sourc. A, Recovery util. environ. effects*, 37(2015) 758 - 765.
- [53] R. Ramakrishnan, K. Kathiravan, K. Sakthivel and T. Sivakumar, *RSC Adv.*, 6 (2016) 45907 - 45922.
- [54] J. Yang, N. Li, S. Li, W. Wang, L. Li, A. Wang, X. Wang, Y. Conga and T. Zhang, *Green Chem.*, 16 (2014) 4879- 4884.
- [55] E. Taarning, I.S. Nielsen, K. Egeblad, R. Madsen, and C. H. Christensen, *ChemSusChem* 1 (2008) 75–78.
- [56]. X. Tong, Z. Liu, L. Yu and Y. Li, *Chem. Commun.*, 51 (2015) 3674-3677.

- [57] F. Pinna, A. Olivo, V. Trevisan, F. Menegazzo, M. Signoretto, M. Manzoli, F. Boccuzzi, *Catal. Today*, 203 (2013) 196–201.
- [58] F. Menegazzo, M. Signoretto, F. Pinna, M. Manzoli, V. Aina, G. Cerrato and F. Boccuzzi, *J. Catal.*, 309 (2014) 241–247.
- [59] F. Menegazzo, T. Fantinel, M. Signoretto, F. Pinna and M. Manzoli, *J. Catal.*, 319 (2014) 61–70.
- [60] O. Casanova, S. Iborra and A. Corma, *J. Catal.*, 265 (2009) 109–116.
- [61] C. Ampelli, K. Barbera, G. Centi, C. Genovese, G. Papanikolaou, S. Perathoner, K. J. Schouten and J. K. Vander Waal, *Catal. Today*, 278(2016) 56–65.
- [62] C. Ampelli, G. Centi, C. Genovese, G. Papanikolaou, R. Pizzi, S. Perathoner, R. J. van Putten, K. J. P. Schouten, A. C. Gluhoi and J. C. van der Waal, *Top Catal.*, 59(2016) 1659–1667.
- [63] K. P. S. Prasad, D. S. Dhawale, T. Sivakumar, S. S. Aldeyab, J. S. M Zaidi, K. Ariga and A. Vinu, *Sci. Technol. Adv. Mater.*, 12 (2011) 044602.
- [64] K.P.S. Prasad, D. S. Dhawale, S. Joseph, C. Anand, M.A. Wahab, A. Mano, C.I. Sathish, V. V. Balasubramanian, T. Sivakumar and A. Vinu, *Microporous Mesoporous Mater.*, 172 (2013) 77–86.
- [65] A. Brindha, K. Kathiravan and T. Sivakumar, *J. Ind. Eng. Chem.*, 36 (2016) 184–193.
- [66] R. Ramakrishnan, S. Kalavani, J. Amala Infant Joice and T. Sivakumar, *Appl. Surf. Sci.*, 258 (2012) 2515–2521.

- [67] Y. Waseda, E. Matsubara and K. Shinoda, X-Ray diffraction crystallography, Springer, 2011.
- [68] S. Jun, S.H. Joo, R. Ryoo, M. Kruk, M. Jaroniec, Z. Liu, T. Ohsuna and O. Terasaki, *J. Am. Chem. Soc.*, 122 (2000) 10712-10713.
- [69] J. Roggenbuck, G. Koch, and M. Tiemann, *Chem. Mater.*, 18 (2006) 4151-4156.
- [70] R. Ryoo, S. H. Joo, M. Kruk and M. Jaroniec, *Adv. Mater.*, 13 (2001) 677-681.
- [71] L.A. Solovyova, A.N. Shmakov, V.I. Zaikovskii, S.H. Joo and R. Ryoo, *Carbon*, 40 (2002) 2477–2481.
- [72] A. Vinu, P. Srinivasu, M. Takahashi, T. Mori, V.V. Balasubramanian, K. Ariga, *Microporous Mesoporous Mater.*, 100 (2007) 20–26.
- [73] A. Vinu and M. Hartmann, *Catal. Today*, 102 – 103 (2005) 189–196.
- [74] A. Vinu, M. Miyahara and K. Ariga, *J. Phys. Chem. B*, 109 (2005) 6436-6441.
- [75] H. Huwe and M. Froba, *Microporous Mesoporous Mater.*, 60 (2003) 151–158.
- [76] B. Ingham, *Crystallogr. Rev.*, 2 (2015) 229-303.
- [77] JCPDS-ICDD, The International Centre for Diffraction Data, 2003.
- [76] V. Valles, B. Ledesma, J. Juarez, M. G. Costa, O. Anunziata and A. Beltramone, *Fuel*, 188 (2017) 155–165.
- [78] V. Meynen, P. Cool and E.F. Vansant, *Microporous Mesoporous Mater.*, 125 (2009) 170–223.

- [79] S.J. Gregg and K.S.W. Sing, Adsorption, Surface Area and Porosity, 2nd ed., Academic Press, London, 1982.
- [80] K. S. W. Sing, D. H. Everett, R. A. W. Haul, L. Moscou, R. A. Pierotti, J. Rouquerol and T. Siemieniewska, International Union of Pure and Applied Chemistry Recommendations, Pure Appl. Chem., 57 (1985) 603-619.
- [81] A. Vinu, M. Miyahara and K. Ariga, J. Phys. Chem. B, 109 (2005) 6436-6441.
- [82] C. Weinberger, S. Haffer, T. Wagner, and M. Tiemann, The Science and Function of Nanomaterials: From Synthesis to Application, ACS Symposium Series, 1/1183 (2014) 3–12.
- [83] H. Li, S. Zhu, H. Xi and R. Wang, Microporous Mesoporous Mater., 89 (2006) 196–203.
- [84] L. Li, Z.H. Zhu, G.Q. Lu, Z.F. Yan and S.Z. Qiao, Carbon, 45 (2007) 11–20.
- [85] H. Huwe and M. Froba, Carbon, 45 (2007) 304–314.
- [86] L. Rivoira, J. Juarez, H. Falcon, M. G. Costa, O. Anunziata and A. Beltramone, Catal. Today, 282 (2017) 123-132.
- [87] B. Karimi, H. M. Mirzaei, H. Behzadnia and H. Vali, ACS Appl. Mater. Interfaces, 7 (2015) 19050–19059.
- [88] J.S.Lee, S.H.Joo and R.Ryoo, Stud. Surf. Sci. Catal., 146(2003) 33-36.
- [89] S. Jun, S. H. Joo, R. Ryoo, M. Kruk, M. Jaroniec, Z. Liu, T. Ohsuna and O. Terasaki, J. Am. Chem. Soc., 122 (2000) 10712-10713.

- [90] J. F. Moulder, W. F. Stickle, P. E. Sobol and K. Bomen, Handbook of x-ray photoelectron spectroscopy, ed. J. Chastain, Perkin-Elmer Corporation (Physical Electronics) 2nd edn., 1992.
- [91] Y. Chen, H. Wang, C. J. Liu, Z. Zeng, H. Zhang, C. Zhou, X. Jia and Y. Yang, *J. Catal.*, 2012, 289 (2012) 105–117.
- [92] S. H. Joo, S. J. Choi, I. Oh, J. Kwak, Z. Liu, O. Terasaki and R. Ryoo, *Nature*, 412 (2001)169-172.

FIGURE CAPTIONS

Fig.1 Small angle X-ray powder diffraction patterns of (a). 1% Au/CMK-3, (b). 3% Au/CMK-3, (c). 5 % Au/CMK-3 and (d). 7 % Au/CMK-3 catalysts.

Fig.2 Wide angle X-ray powder diffraction patterns of (a). 1% Au/CMK-3, (b). 3% Au/CMK-3, (c). 5 % Au/CMK-3 and (d). 7 % Au/CMK-3 catalysts.

Fig.3 XPS spectra of Au4f (Au 4f_{7/2} & Au 4f_{5/2}) core levels of the catalysts a). 1% CMK-3, (b) 3 Au/CMK-3, (c) 5 % Au/CMK-3 and (d). 7 % Au/CMK-3.

Fig. 4 HR-SEM micrographs of SBA-15 with (a). low magnification, (b). high magnification and (c). CMK-3 with low magnification and (d). CMK-3 with high magnification.

Fig.5 HR-SEM micrographs of (a). 5% Au/CMK-3, (b). 7% Au/CMK-3, (c). 5% Au/CMK-3 with high magnification and (d). EDS data of 5% Au/CMK-3 catalysts.

Fig.6 HR-TEM micrographs of (a). 5% Au/CMK-3, (b). 7% Au/CMK-3 and high magnification images of (c). 5% Au/CMK-3, (d). 7% Au/CMK-3, (e). Particle size distribution of 5% Au/CMK-3 (f). Lattice fringes of 5% Au/CMK-3 catalysts.

Fig.7 (a) HR-TEM micrographs of spent 5% Au/CMK-3 catalyst after 5 catalytic cycles and (b). Particle size distribution of spent 5% Au/CMK-3 catalyst.

Fig.8 FT-IR spectra of 5% Au/CMK-3 spent catalyst (a). at 393 K, O₂ (15 bar) (b). along with TBHP at 393 K and (c). at 413 K.

FIGURES

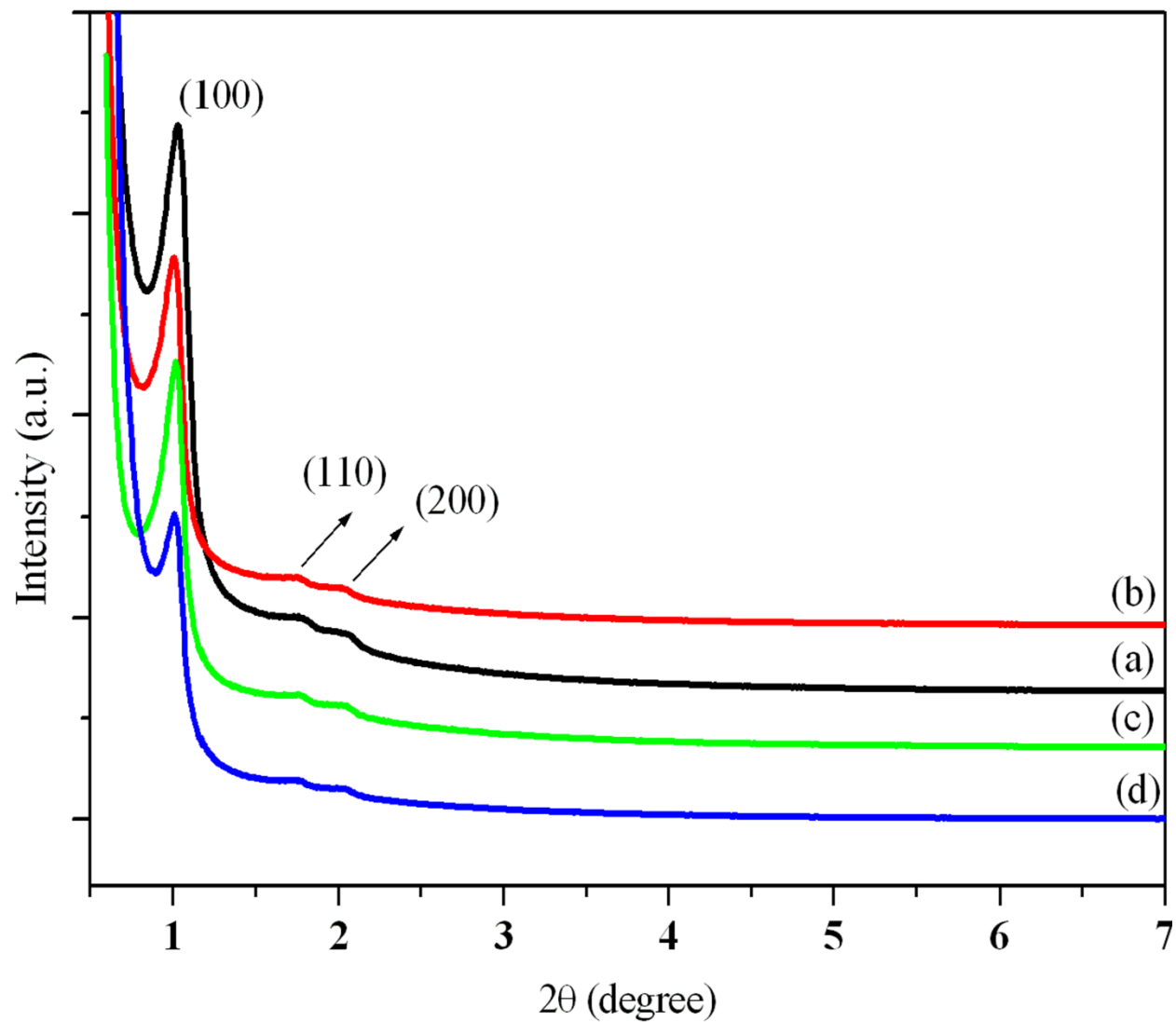


Fig. 1 Small angle X-ray powder diffraction patterns of (a). 1% Au/CMK-3, (b). 3% Au/CMK-3, (c). 5 % Au/CMK-3 and (d). 7 % Au/CMK-3 catalysts.

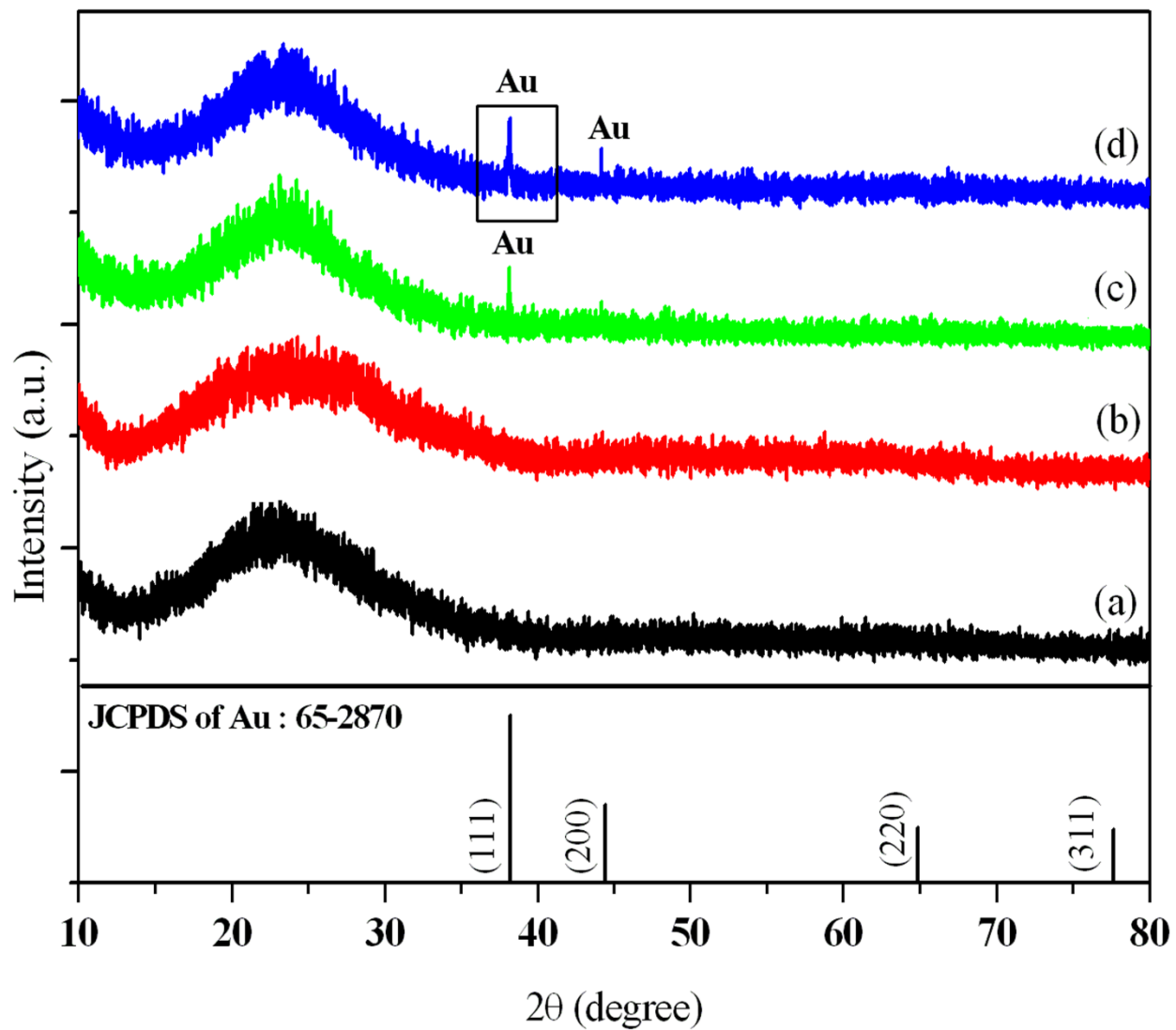


Fig. 2 Wide angle X-ray powder diffraction patterns of (a). 1% Au/CMK-3, (b). 3% Au/CMK-3, (c). 5 % Au/CMK-3 and (d). 7 % Au/CMK-3 catalysts.

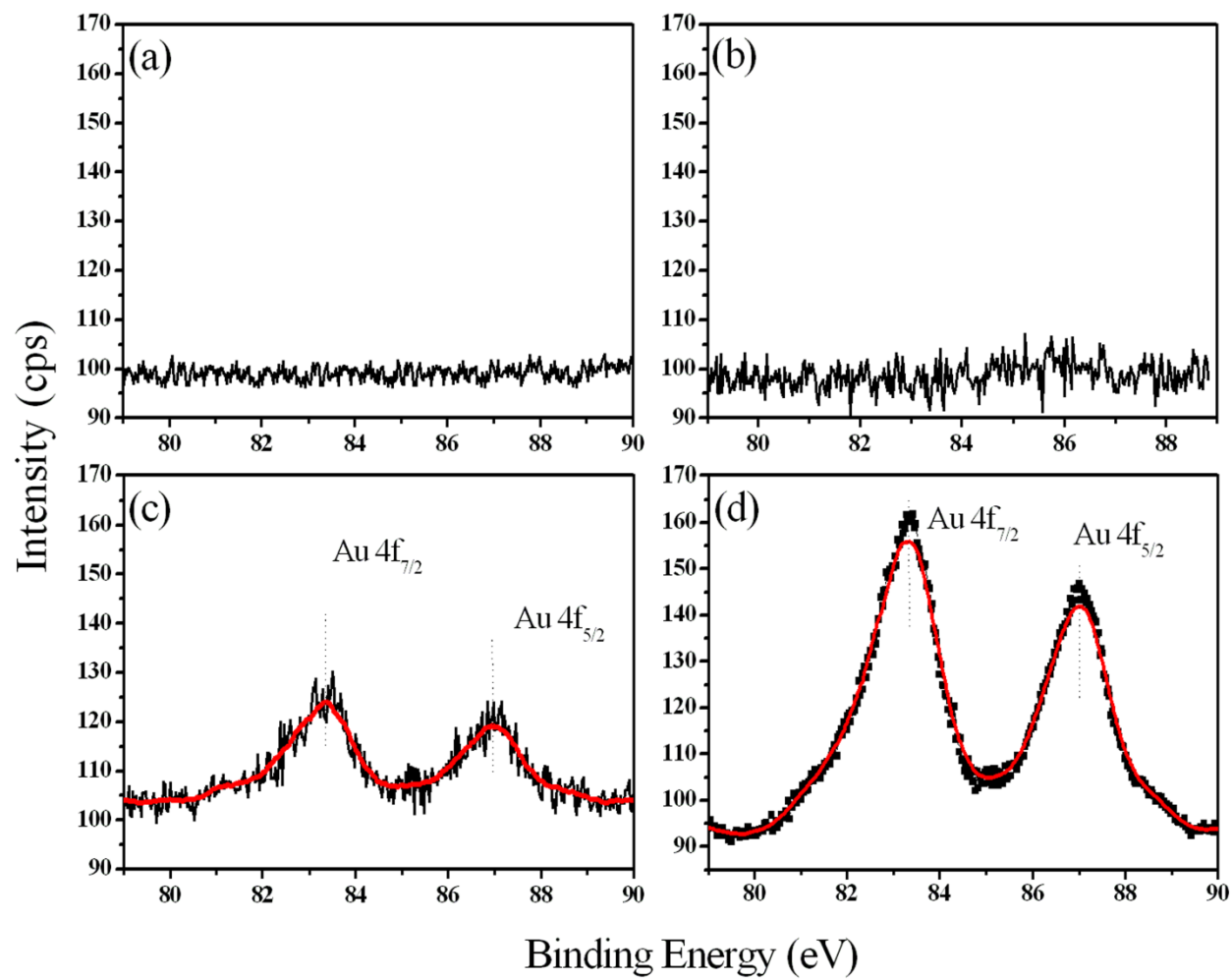


Fig. 3 XPS spectra of Au4f (Au 4f_{7/2} & Au 4f_{5/2}) core levels of the catalysts a). 1 % CMK-3, (b) 3 % Au/CMK-3, (c) 5 % Au/CMK-3 and (d). 7 % Au/CMK-3.

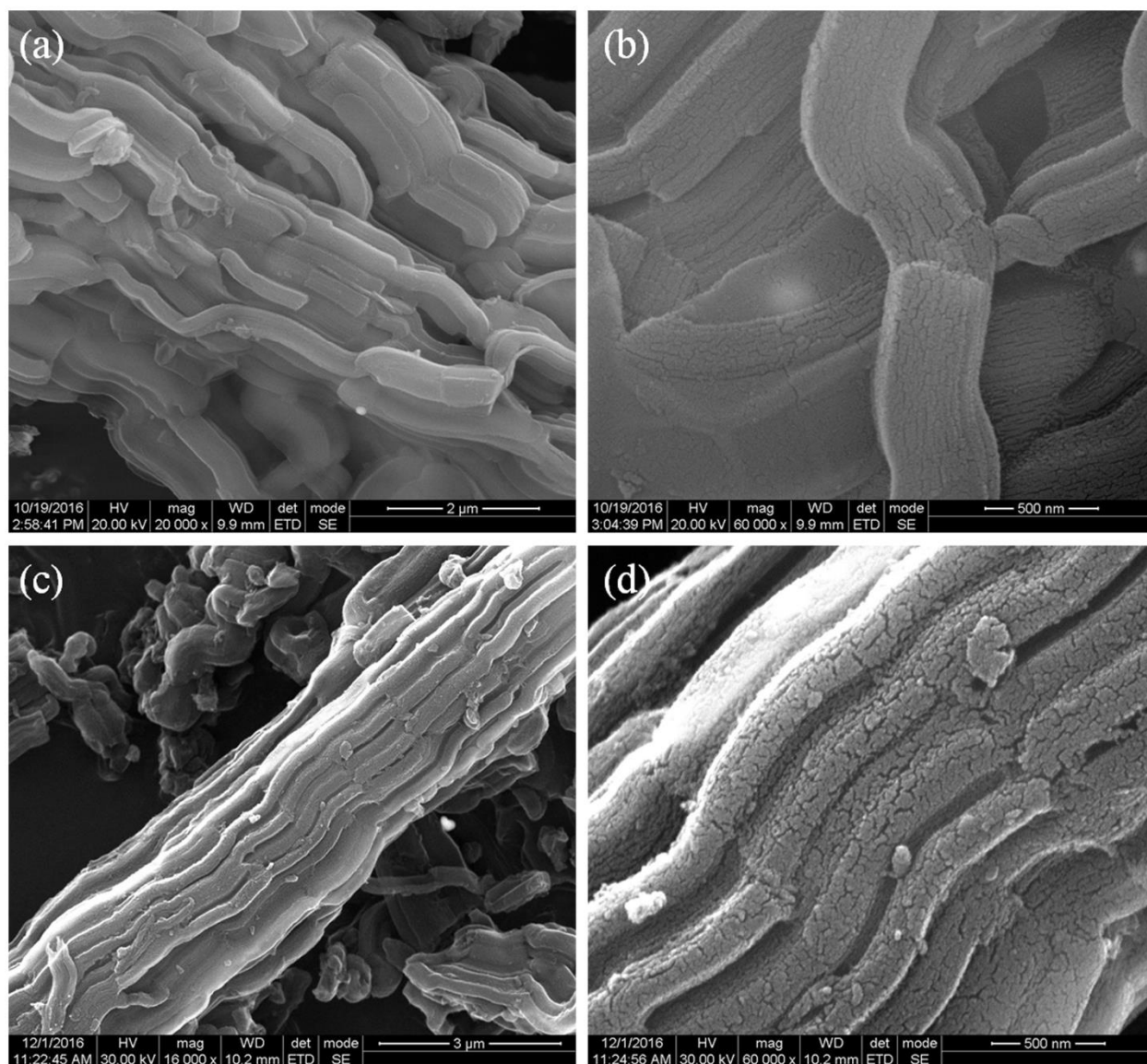


Fig. 4 HR-SEM micrographs of SBA-15 with (a). low magnification, (b). high magnification and (c). CMK-3 with low magnification and (d). CMK-3 with high magnification.

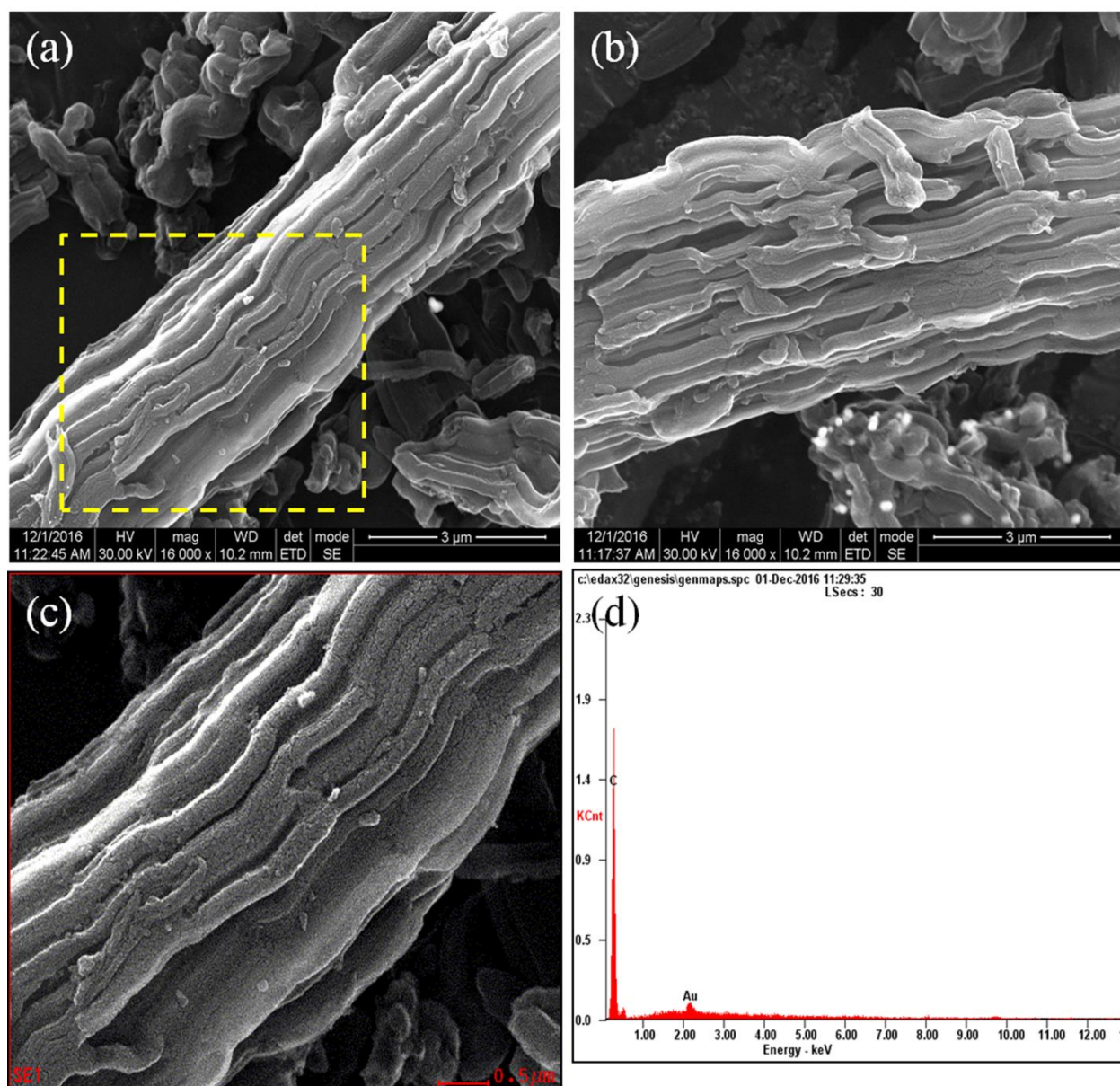


Fig. 5 HR-SEM micrographs of (a). 5% Au/CMK-3, (b). 7% Au/CMK-3, (c). 5% Au/CMK-3 with high magnification and (d). EDS data of 5% Au/CMK-3 catalysts.

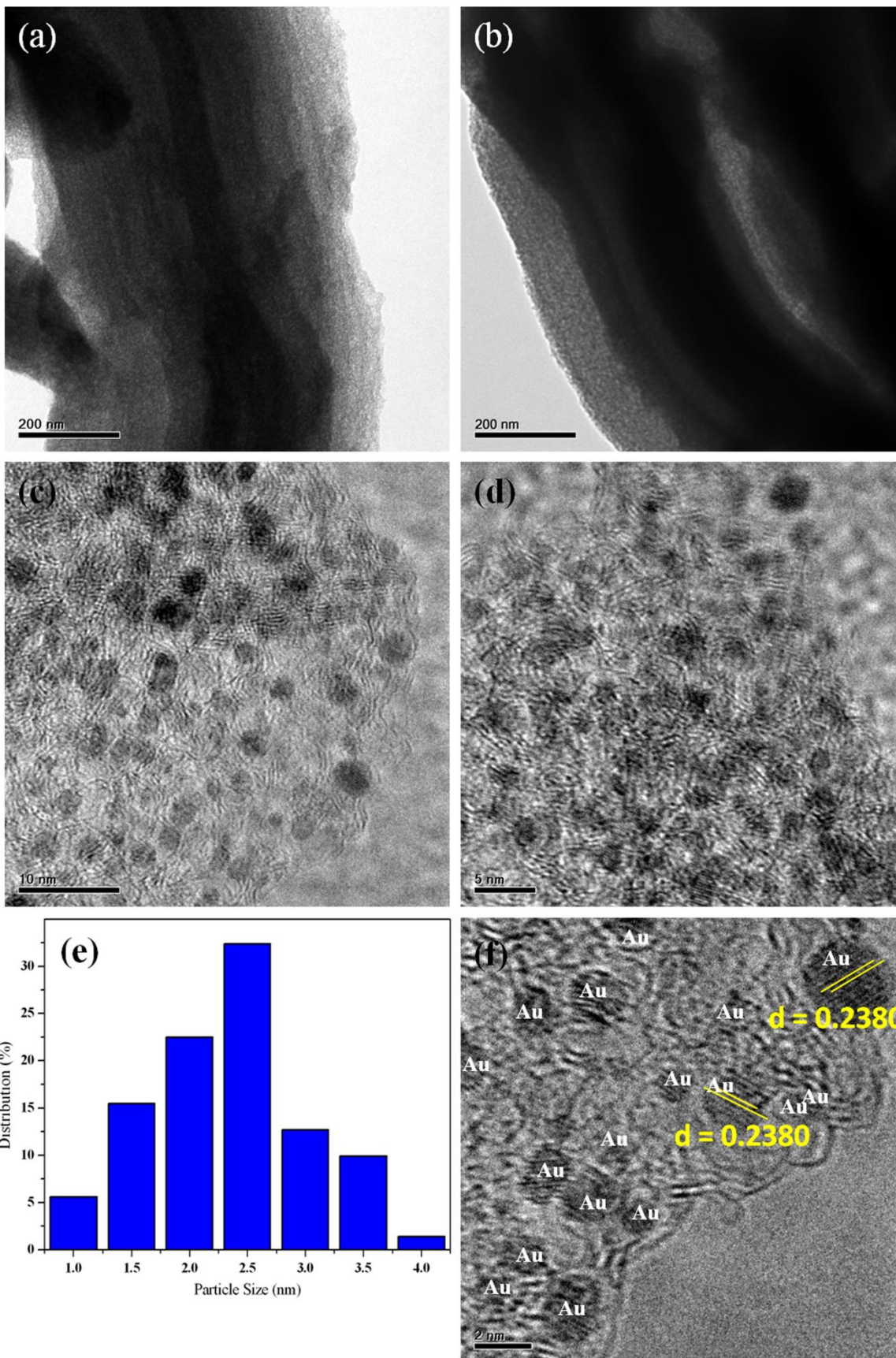


Fig. 6 HR-TEM micrographs of (a). 5% Au/CMK-3, (b). 7% Au/CMK-3 and high magnification images of (c). 5% Au/CMK-3, (d). 7% Au/CMK-3, (e). Particle size distribution of 5% Au/CMK-3 and (f). Lattice fringes of 5% Au/CMK-3 catalyst.

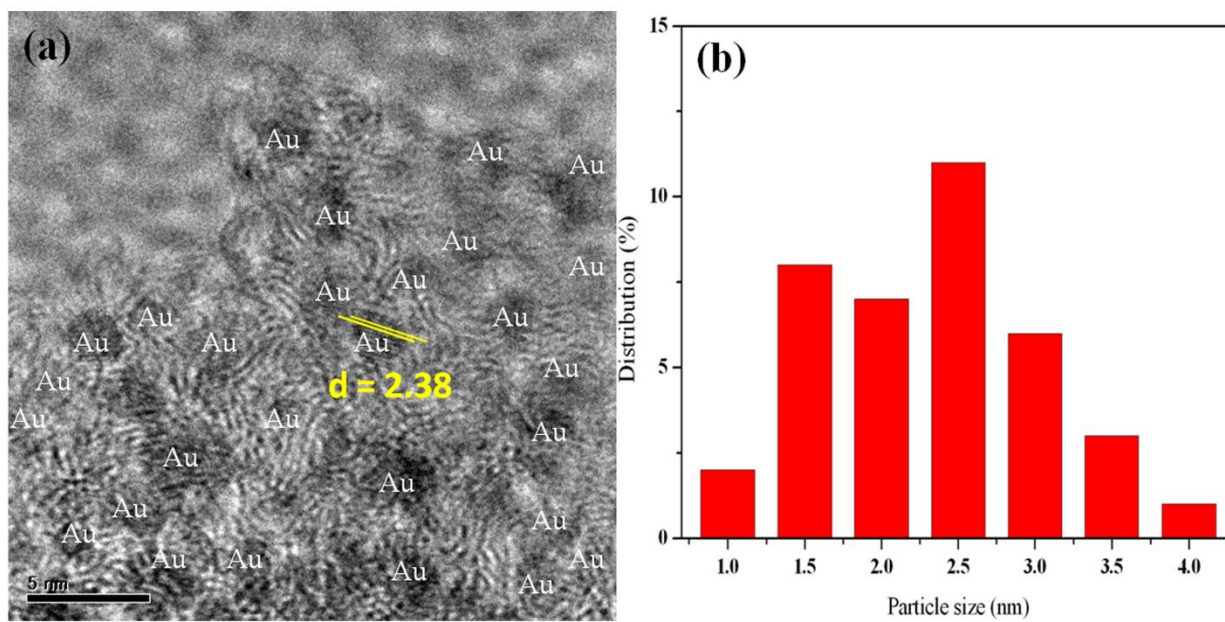


Fig.7 (a) HR-TEM micrographs of spent 5% Au/CMK-3 catalyst after 5 catalytic cycles and (b). Particle size distribution of spent 5% Au/CMK-3 catalyst.

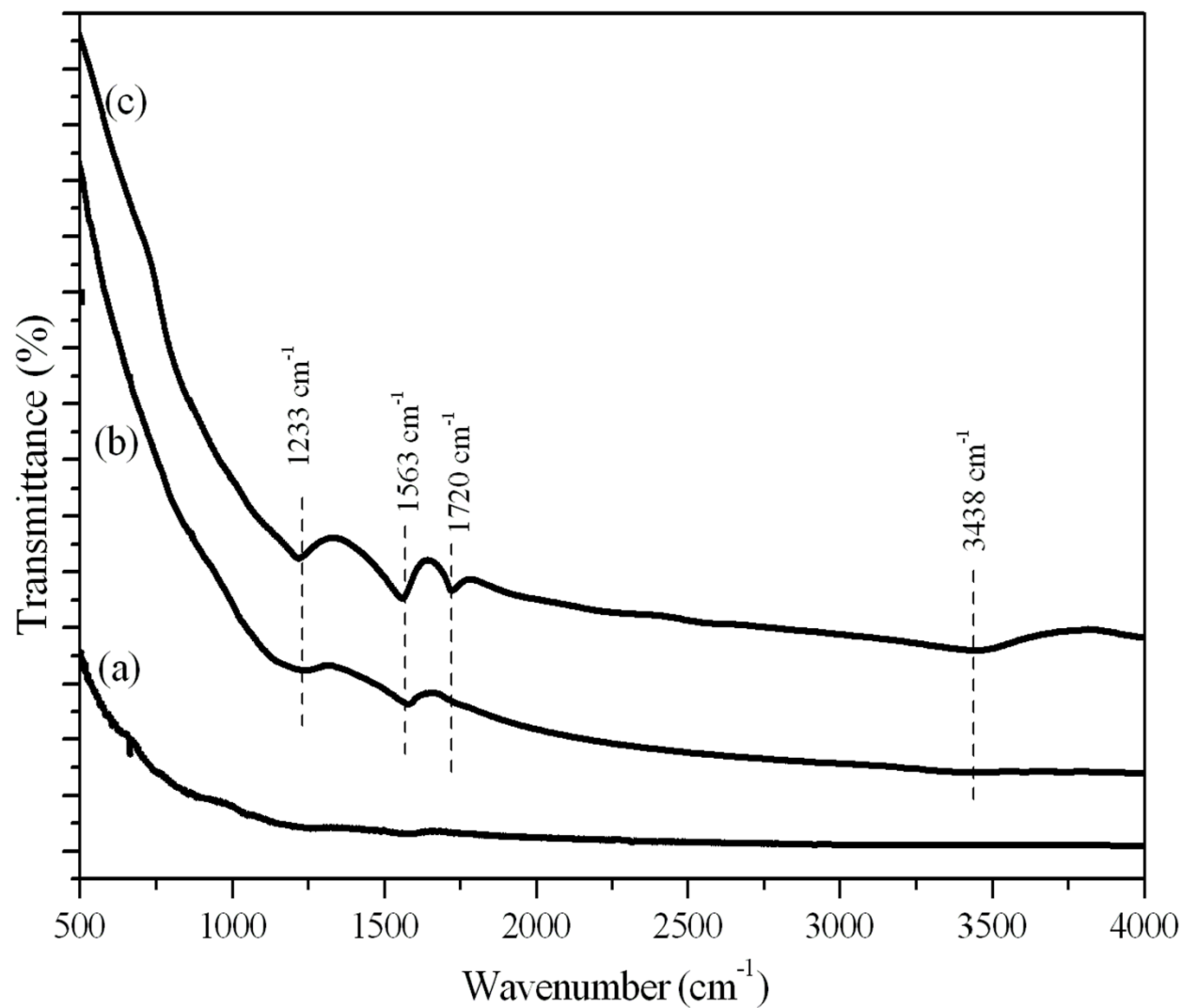
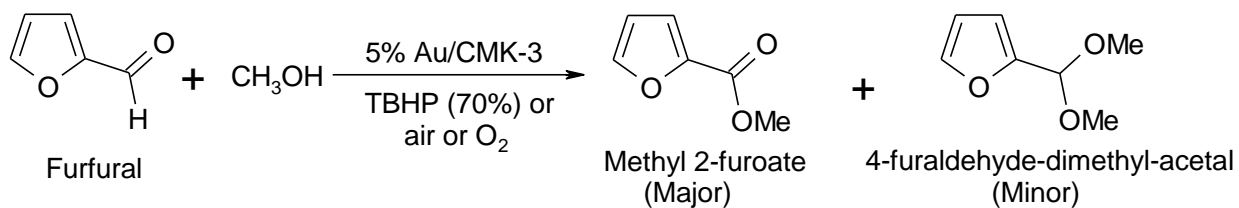


Fig. 8 FT-IR spectra of 5% Au/CMK-3 spent catalyst (a). at 393 K, O₂ (15 bar) (b). reaction carried out along with TBHP at 393 K and (c). at 413 K.



Scheme.1 Oxidative esterification of furfural to methyl 2-furoate.

TABLE CAPTIONS

Table.1 Texture parameters and Au contents of the synthesized catalysts.

Table.2 Catalytic oxidative esterification of furfural over various catalysts.

Table.3 Effect of Au content on the catalytic activity.

Table.4 Optimization of reaction temperature.

Table.5 Optimization of reaction time.

Table.6 Effect of various bases.

Table.7 Effect of oxidants.

Table.8 Reusability test of 5% Au/CMK-3.

TABLES

Table.1 Texture parameters and Au contents of the synthesized catalysts.

Catalyst	d_{100}	a_0	S_{BET}	V_P	d_p	CWT	Au content (Wt. %)				Au metal cluster average size (nm)	
	(nm) ^a	(nm) ^b	(m ² /g) ^c	(cm ³ /g) ^d	(nm) ^e	b(nm) ^f	Actual	ICP	EDS	XPS	XRD	HR-TEM
SBA-15	9.20	10.62	740	1.54	7.69	2.70	-	-	-	-	-	-
CMK-3	8.60	9.93	1096	1.03	4.56	5.73	-	-	-	-	-	-
1% Au/CMK-3	8.74	10.09	1039	0.97	4.10	5.99	1	0.92	-	-	-	-
3% Au/CMK-3	8.74	10.09	965	0.92	4.10	5.99	3	2.89	-	-	-	-
5% Au/CMK-3	8.65	9.99	903	0.88	3.90	6.00	5	4.90	2.13	1.87	2.3	2.5
7% Au/CMK-3	8.57	9.89	880	0.81	3.80	6.09	7	6.85	4.68	3.25	2.5	2.4

^a d_{100} calculated from the x-ray diffraction pattern from (100) plane.

^bUnit cell size calculated using the formula, $a_0=2d_{100}/\sqrt{3}$.

^cSurface area calculated from BET equation at P/P₀ range of 0.05 to 0.3

^dTotal pore volume calculated at P/P₀ = 0.98.

^ePore diameter calculated from the adsorption branch of the isotherm- BJH

^fCarbon Wall thickness (CWT) calculated using, $b = a_0 - d_p$.

Table.2 Catalytic oxidative esterification of furfural over various catalysts.

Catalysts	Conversion (%)	Selectivity (%)	
		Methyl 2-furoate	4-furaldehyde-dimethyl-acetal
Au/CMK-3	77.7	96.8	3.2
Pd/CMK-3	80.0	92.3	7.7
Pt-CMK-3	60.4	87.7	12.3
Ni/CMK-3	29.1	100	-
Au/SBA-15	73.0	99.8	0.2
Au/Graphite	76.3	87.2	12.8
Au/Graphene	40.7	85.4	14.6
Au/MWCNT	72.6	93.3	6.7
Au/Activated C	27.4	98.8	1.2
Au/TiO ₂	93.9	79.6	20.4

Reaction conditions:

Furfural- 300 μ l, TBHP- 3eq. 50 mg of catalyst: Metal loading content – 5 wt. %, 20 ml of CH₃OH, Reaction temperature-393 K and Reaction time – 3 hr.

Table.3 Effect of Au content on the catalytic activity.

Catalyst	Conversion (%)	Selectivity (%)	
		Methyl 2-furoate	4-furaldehyde-dimethyl-acetal
1% Au/CMK-3	49.7	98.1	1.9
3% Au/CMK-3	68.9	97.4	2.6
5% Au/CMK-3	77.7	96.8	3.2
7% Au/CMK-3	79.5	96.5	3.5

Reaction conditions:

Furfural- 300 μ l, TBHP- 3eq. 50 mg of catalyst, 20 ml of CH₃OH, Reaction temperature – 393 K and Reaction time – 3 hr.

Table.4 Optimization of reaction temperature.

Reaction Temperature (K)	Conversion (%)	Selectivity (%)	
		Methyl 2-furoate	4-furaldehyde- dimethyl-acetal
333	23.5	98.5	1.5
353	53.7	97.3	1.7
373	66.9	97.7	2.4
393	77.7	96.8	3.2
413	74.9	90.8	9.2

Reaction conditions:

Furfural- 300 μ l, TBHP- 3eq., 50 mg of catalyst of 5 wt. % Au/CMK-3, 20 ml of CH₃OH and Reaction time – 3 hr.

Table.5 Optimization of reaction time.

Reaction time (hr)	Conversion (%)	Selectivity (%)	
		Methyl 2-furoate	4-furaldehyde-dimethyl-acetal
1	12.6	99.7	0.3
2	55.7	98.0	2.0
3	77.7	96.8	3.2
4	82.6	91.0	9.0
5	85.1	88.3	11.7

Reaction conditions:

Furfural- 300 μ l, TBHP- 3eq., 50 mg of catalyst of 5 wt. % Au/CMK-3, 20 ml of CH₃OH and Reaction temperature-393K.

Table.6 Effect of various bases.

Base	Conversion (%)	Selectivity (%)	
		Methyl 2-furoate	4-furaldehyde-dimethyl-acetal
NaOH	52.0	94.8	5.4
NaOCH ₃	55.7	99.0	1.0
K ₂ CO ₃	50.0	99.0	1.0
Li ₂ CO ₃	73.4	87.3	12.9
Cs ₂ CO ₃	79.0	90.9	9.1

Reaction conditions:

Furfural- 300 μ l, O₂ – Pressurized from rubber bladder, 50 mg of catalyst of 5 wt. % Au/CMK-3, 20 ml of CH₃OH and Reaction temperature-393K.

Table.7 Effect of oxidants

Oxidants	Reaction pressure (bar)	Conversion (%)	Selectivity (%)	
			Methyl 2-furoate	4-furaldehyde-dimethyl-acetal
Air	Ambient	0	0	0
Air	5	79.0	99.0	1.0
Air	10	85.7	98.7	1.3
Air	15	90.1	99.1	0.9
TBHP	-	77.7	96.8	3.2
Air + TBHP	10	95.7	90.1	9.9
O ₂ + TBHP	10	91.5	99.0	1.0
Oxygen	5	78.6	99.0	1.0
Oxygen	10	86.0	99.0	1.0
Oxygen	12	95.7	99.0	0.1
Oxygen	15	99.7	99.6	0.4

Reaction conditions:

Furfural- 300 μ l, 50 mg of catalyst of 5 wt. % Au/CMK-3, 20 ml of CH₃OH, Reaction temperature-393K and Reaction time – 3 hr.

Table.8 Reusability test of 5% Au/CMK-3

Catalyst	Catalytic recycle	Conversion (%)	Selectivity (%)	
			Methyl 2-furoate	4-furaldehyde- dimethyl-acetal
Au/CMK-3	1	99.7	99.3	0.7
Au/CMK-3	2	99.2	98.8	1.2
Au/CMK-3	3	99.8	98.7	1.3
Au/CMK-3	4	98.2	99.9	0.1
Au/CMK-3	5	95.0	99.7	0.3

Reaction Conditions:

Furfural – 300 ml, O₂ (15 bar), 50 mg of catalyst of 5 wt. % Au/CMK-3, 20 ml of CH₃OH,
Reaction temperature – 393 K and Reaction time – 3 h.